Predicting Carpal Bone Kinematics Using an Expanded Digital Database of Wrist Carpal Bone Anatomy and Kinematics

Bardiya Akhbari [iD],[1] Douglas C. Moore [iD],[2] David H. Laidlaw [iD],[3] Arnold-Peter C. Weiss,[2] Edward Akelman,[2] Scott W. Wolfe,[4] Joseph J. Crisco [iD][1,2]

[1]Center for Biomedical Engineering and School of Engineering, Brown University, Providence, Rhode Island, 02912, [2]Department of Orthopedics, The Warren Alpert Medical School of Brown University and Rhode Island Hospital, Providence, Rhode Island, 02903, [3]Department of Computer Science, Brown University, Providence, Rhode Island, 02912, [4]Hand and Upper Extremity Center, Hospital for Special Surgery and Weill Medical College of Cornell University, New York, New York, 10021

ABSTRACT: The wrist can be considered a 2 degrees-of-freedom joint with all movements reflecting the combination of flexion–extension and radial–ulnar deviation. Wrist motions are accomplished by the kinematic reduction of the 42 degrees-of-freedom of the individual carpal bones. While previous studies have demonstrated the minimal motion of the scaphoid and lunate as the wrist moves along the dart-thrower's path or small relative motion between hamate-capitate-trapezoid, an understanding of the kinematics of the complete carpus across all wrist motions remains lacking. To address this, we assembled an open-source database of in vivo carpal motions and developed mathematical models of the carpal kinematics as a function of wrist motion. Quadratic surfaces were trained for each of the 42-carpal bone degrees-of-freedom and the goodness of fits were evaluated. Using the models, paths of wrist motion that generated minimal carpal rotations or translations were determined. Model predictions were best for flexion–extension, radial–ulnar deviation, and volar–dorsal translations for all carpal bones with $R^2 > 0.8$, while the estimates were least effective for supination-pronation with $R^2 < 0.6$. The wrist path of motion's analysis indicated that the distal row of carpal bones moves rigidly together (<3° motion), along the anatomical axis of wrist motion, while the bones in the proximal row undergo minimal motion when the wrist moves in a path oblique to the main axes. The open-source dataset along with its graphical user interface and mathematical models should facilitate clinical visualization and enable new studies of carpal kinematics and function. © 2019 Orthopaedic Research Society. Published by Wiley Periodicals, Inc. J Orthop Res 37:2661–2670, 2019

Keywords: wrist motion; carpal kinematics; kinematics modeling; open-source database; carpal database

The wrist joint can be considered a 2 degrees-of-freedom (DOF) joint with all movements reflecting combinations of flexion–extension (FE) and radial-ulnar (RU) deviation. These two DOFs are accomplished by kinematic reduction of the 42 DOFs of seven carpal bones. The pisiform, while identified as a carpal bone, is not considered a significant factor as it has a minimal role in wrist kinematics.[1] The passive motion and the reduction in the DOFs is due to the minimal direct tendon and muscular insertions to carpal bones.[2,3] Carpal bone motion is thus driven by the contact forces from their distal structures (i.e., metacarpals), proximal structures (i.e., triangular fibrocartilage complex and radius),[2] and their surrounding ligamentous constraints.[4,5]

To describe the carpal bone motion patterns, two major kinematic theories of *row* and *column* have been proposed.[6] Although the row theory (describing the distinct motion patterns for proximal and distal carpal rows),[7–11] column theory (assuming three medial-central-lateral carpal columns as an inner mechanism for the wrist motion),[12,13] and their combinations[14,15] have helped in devising and evaluating clinical procedures,[16] they are not predictive or specific about individual carpal bone kinematics within the overall wrist motion.

Most previous studies have focused on individual carpal bone or groups of two/three bones during specific

wrist motions such as FE, RU, or the dart thrower's motion (DTM).[13,17–21] While these studies have demonstrated how individual bones move relative to each other—importantly, the minimal motion of scaphoid and lunate in the DTM[19]—or how a group of carpal bones moves relative to each other (e.g., small relative motion between hamate, capitate, and trapezoid),[13] the ability to comprehensively model the entire carpus as a function of wrist motion (FE and RU; 2 DOF) could help us to better understand the wrist function. Such a model could also illuminate how individual carpal bone kinematics are altered after an injury, or how to study the biomechanics of total wrist arthroplasty designs, which currently reduce the wrist to a two-DOF joint.[22]

A model's success is assessed by its ability to predict data from a large dataset that the model has not seen.[23] Thus far, a predictive model for the carpal bones has not been developed, perhaps in part because of the lack of a detailed kinematic database. Previous attempts at constructing a predictive and informative model of carpal bone motion have been primarily based on radiographic or cadaveric observations.[6,16,24,25] Due to the variations in motion patterns of the carpal bone articulations among wrists and lack of large sample sizes, none of these models have been rigorously evaluated for predictive ability. Recently, a stable central column theory[26] of carpal bones was proposed by modeling the isometry of ligament lengths on an in vivo dataset, however, the study was limited to a single specific task (in RU direction) with a small sample size

Correspondence to: Joseph J. Crisco (T: (401) 444-4231; F: (401) 444-4418; E-mail: joseph_crisco@brown.edu)

(10 wrists). Computational modeling and finite element analysis are powerful tools for evaluating wrist contact forces in mostly static postures,[27–29] however, to date, they have not been used for kinematic analysis and prediction.

Previously, our group published a database of in vivo carpal kinematics and anatomy for 60 healthy wrists.[19,30–33] We postulate that expanding the database with additional studies[34–39] would provide a more complete picture of carpal kinematics. In this study, our first aim was to assemble and describe an expanded open-source database of in vivo wrist motions from 120 previously studied wrists. Using the database, our second aim was to develop a mathematical model of carpal kinematics as a function of two wrist flexion-extension and radioulnar deviation to predict individual carpal bone kinematics. Our third aim was to use the model to determine paths of wrist motion that result in minimal carpal bone movement. In addition, a graphical user interface (GUI) of the database and the mathematical model were developed to enable investigators to qualitatively and quantitively observe the wrist motions available in the database and build upon the proposed mathematical models.

METHODS
Overview
This study has integrated data from four NIH-funded computed tomography (CT)-image based in vivo studies on the wrist and thumb kinematics.[30,34–39] The database used in this study has been also made freely available through SimTk.org (https://simtk.org/projects/carpal-database). The current database includes CT-derived carpal bone models from 90 healthy subjects (120 wrists) and carpal bone kinematics in 1,215 unique wrist positions (Table 1 and Fig. 1).

Database Description—Data Acquisition
Healthy subjects were recruited after institutional review board approval and were all pre-screened for a history of wrist injuries by board-certified orthopedic hand surgeons. Data from 30 subjects has been described in detail previously (Table 1).[30] The expanded database contains data from an additional 60 subjects: 14 of which were studied in extreme wrist flexion, extreme wrist extension, and five positions along the path of DTM. Forty-six of these participants were in a study of carpometacarpal joint biomechanics, in which the thumb and wrist were in various poses (thumb neutral pose, adduction, abduction, flexion, extension, jar twist, jar grasp, and key pinch)[40] (Table 1). The neutral pose was defined by aligning the dorsum of the third metacarpal with the forearm's dorsal surface using a goniometer in functional, combined, and incremental orthogonal cohorts.[30] In the CMC cohort, the neutral position was defined using a splint placing the wrist in an anatomic neutral posture (approximately 0° flexion/extension and ulnar/radial deviation).[41] Two subjects (four wrists) neutral position did not follow the CT scan acquisition protocol, thus they were excluded for mathematical modeling.

The bone surface models have been constructed from the CT scans (Lightspeed 16; GE Medical, Milwaukee, WI) that were obtained of the wrist in the aforementioned poses.[30,42]

The CT scan resolutions differed between the datasets and ranged from 0.2×0.2 to 0.4×0.4 mm^2 in the transverse plane of the hand, and 0.625 to 1 mm along the axis of the forearm. Digital models of the outer cortical surface of radius, ulna, carpal bones, and metacarpals were obtained from the neutral posture CT images using Mimics v12–19 (Materialize, Leuven, Belgium) by employing thresholding and edge detection algorithms. No cartilage was modeled from the CT images.

Database Description—Data Analysis
Kinematic transformations were calculated from the neutral wrist position to each target position using a tissue-classified distance fields algorithm to register the bones in the neutral position to all other posture's CT scans, creating six-DOF global transformations from the neutral scan to each subsequent position as described before.[43] Using the bones' inertial properties, an orthogonal coordinate system for each carpal bone was constructed with the origin at the bone models' volumetric centroid (bone's inertial coordinate system [ICS], Supplementary Fig. S1).[32]

A radial coordinate system (RCS) was calculated based on the modification of the International Society of Biomechanics (ISB) recommendation and the distal radius' anatomical landmarks (Fig. 2).[20,44,45] The x-axis direction was defined by the central axis of the distal radius shaft. The y-axis was defined as a line perpendicular to the x-axis, originating from the center of the sigmoid notch and exiting at the metaphyseal flare of the radius, and transposed proximally to the radial articular surface. The z-axis was the cross product of the other axes. The origin was the projection of the intersection of the x-axis direction and y-axis direction on the distal radius surface.

The database and wrist motion in all postures can be observed and evaluated both qualitatively and quantitatively by the GUI provided with the database. Written with MATLAB 2018b (The MathWorks, Natick, MA), the GUI enables users to investigate the position and rotation of the carpal bones in any wrist motion available in the database on an average male or female bone model. Users are also capable of importing subject-specific bone models (captured at the neutral position) to observe the wrist motions available on the database on their imported three-dimensional models.

Carpal Bones Motion in the RCS
Wrist motion was defined in terms of the FE and RU of the capitate bone (CAP) because it has been previously shown that the capitate moves almost identically to the third metacarpal.[33] The 6-DOF kinematics of the scaphoid (SCA), lunate (LUN), triquetrum (TRQ), trapezium (TPM), trapezoid (TPD), and hamate (HAM) were described as a function of the wrist motion.

The motion of each carpal bone was calculated in the RCS with respect to the neutral pose and described with the helical axis of motion (HAM) parameters. HAM parameters characterize the motion as a single rotation (ϕ) about and translation along the unique screw axis (Fig. 2). The rotational components of the bone motion were decomposed using ϕ angle and the screw axis's orientation to construct supination-pronation (SP), FE, and RU angular components. Translations were defined as the displacement of the origin of bone's ICS in the RCS in the distal-proximal (distal-proximal translation [DPT]), radial-ulnar (RUT), and volar-dorsal directions (VDT). Translations were scaled by the cube root of capitate volume to eliminate the influence of bone size.[46]

Table 1. Breakdown of Our Open-Source Carpal Database

Group	Description	Gender		Age		Wrist		# Postures
		Male (M)	Female (F)	Young (<45 years)	Old (>45 years)	Left	Right	
CMC Cohort[34,40,41]	CMC joint in this study has different poses; however, the wrist motion was unconstrained	21	25	21 (10 M, 11 F)	25 (11 M, 14 F)	10	36	530
Functional Cohort[35–39]	Wrists were tested in five hammering tasks, extreme flexion, and extreme extension tasks	7	7	14	–	–	14	165
Combined Cohort[30–33]	Wrists were tested in specific anatomical ROM poses and DTM tasks	10	10	20	–	20	20	360
Incremental Orthogonal Cohort[30–33]	Wrists were tested in anatomical ROM tasks	5	5	10	–	10	10	160
TOTAL #		43	47	65	25	40	80	**1215**

Forty-six wrists of 46 healthy subjects in a study of carpometacarpal (CMC) joint from 2012 to 2015, 14 wrists of 14 healthy subjects from 2008 to 2010, and 60 healthy wrists (30 subjects, for both sides) from 2000 to 2006. The total number of unique wrist postures was 1,215 (120 neutral, 1,095 others). Subjects who were younger than 45 years were categorized as a young-age group and the rest were categorized in the old age group.

Mathematical Modeling

To create a predictive relationship between the wrist and carpal motion, the mathematical models were constructed on a training set and then were evaluated on a test set. Before modeling, the datasets from 20 subjects (30 wrists, 259 wrist motions) were randomly selected and held out to assess the accuracy of the mathematical models (test set). If the subject had bilateral data, the data from both sides were included in the test set to remove any biases in the selection. The datasets of the remaining 68 subjects (86 wrists, 804 wrist motions) were used for training the model (Fig. 3). In total, the carpal kinematics for 116 wrists from 88 subjects in a total of 1,179 wrist postures, which resulted in 1,063 calculated motions (i.e., # of total postures—# of neutral poses) were used for mathematical modeling.

For each carpal bone DOF ($Bone_{DOF}$), a second-order quadratic surface with the independent variables of wrist FE and RU (CAP_{FE} and CAP_{RU}) were constructed (Equation (1)):

$$Bone_{DOF} = p10 \times CAP_{RU} + p01 \times CAP_{FE} + p20 \times CAP_{RU}^2$$
$$+ p11 \times CAP_{RU} \times CAP_{FE} + p02 \times CAP_{FE}^2 \qquad (1)$$

where $p10$, $p01$, $p20$, $p11$, and $p02$ are the coefficients of the quadratic surface. The quadratic surface equation was used to improve the predictions at the extreme of motions. Higher-order polynomials were not used because they resulted in overfitting and unnatural behavior of the bone motions. A cross-validation technique with a leave-one-out strategy was performed on the training set, and the coefficients were calculated using the least-squares method in each iteration. The best model was selected as the model with the lowest root-mean-squared-error (RMSE) in the cross-validation procedure. The database' kinematics and mathematical models were visualized using Delaunay triangulation[47] of every 3D data point (CAP_{FE}, CAP_{RU}, $Bone_{DOF}$), color-coded by the magnitude of that DOF rotation/translation. The face color of Delaunay triangles was the average of the value for each vertex of the triangle for an interpretable visualization.

To explore carpal kinematics predicted by the models, we sought to identify paths of wrist motion along which carpal DOFs were minimal (MM wrist paths). For instance, the path of wrist motion that generates minimal FE movement for the scaphoid was identified as the MM wrist path for SCA_{FE}. The MM wrist paths were calculated numerically using grid-points limited by the minimum and maximum ranges of our dataset (90° extension, 120° flexion, 40° radial deviation, 60° ulnar deviation) with an interval of 0.5°.

Statistical Analysis

The generalizability of the models (i.e., how well each model predicts the motion of carpal bones from a test set) was evaluated by R^2, RMSE, and the average of model's error on the test set (randomly selected 30 wrists). As R^2 and RMSE can be statistically biased,[23] wrist motions were separated into octants based on the relationship of wrist FE and RU rotation angles for further analysis of the behavior of the generated model in different regions of wrist motion. The histograms of differences were assessed in each octant of RU and FE by measuring the mean and standard deviation of errors.
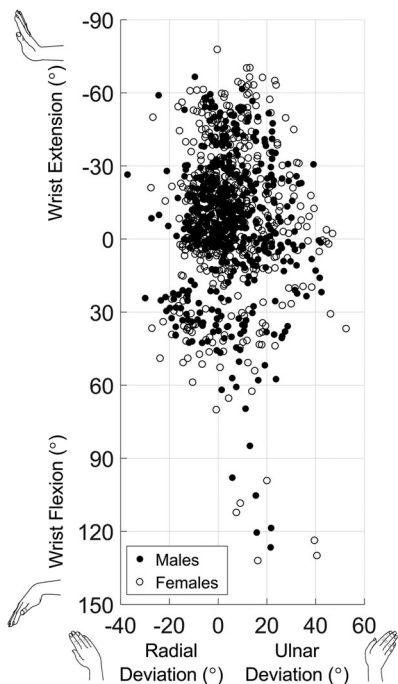
Figure 1. Wrist motions within the carpal dataset for all 120 wrists. Wrist motion was defined as the motion of capitate in the radial coordinate system, and each point depicts the motion of the wrist in a single task.

To analyze and compare the patterns of MM wrist paths for the carpal bone DOFs, linear regression ($p < 0.05$) was used to calculate the lower and upper confidence intervals (LCI and UCI) of the MM wrist path's slope on a plot of wrist motion. The slope demonstrates the ratio of the wrist's FE and wrist's RU when the carpal bone moves only minimally. The MM wrist paths that did not follow a linear pattern were described by points along a curve based on the wrist FE or RU.
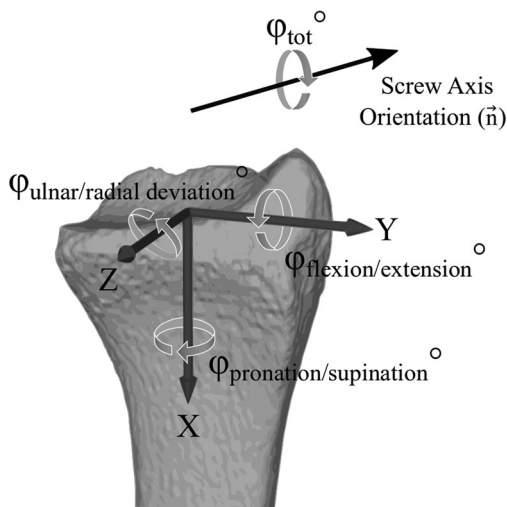

Figure 2. Radial coordinate system and the helical axis of motion parameters. n is a vector defining the orientation of the screw axis (n_x, n_y, n_z) and ϕ_{tot} is the rotation about the axis. This angle can be decomposed into rotational components ($\phi_{tot}.n_x$, $\phi_{tot}.n_y$, $\phi_{tot}.n_z$).

RESULTS

The published database (https://simtk.org/projects/carpal-database) includes CT-generated carpal bone anatomy models from 90 healthy subjects (120 wrists) and the carpal bone kinematics in 1,215 unique wrist positions from four NIH-funded studies. A GUI was also developed to maximize user interaction with this database and the mathematical model constructed in this study (Supplementary Documents).

The mathematical models (42 models) performed well on the 30 held-out wrists (test set) in predicting FE ($R^2 > 0.9$ and RMSE < 6.0°) for all carpus bones (Table 2). The models also performed well for RU ($R^2 > 0.6$ and RMSE < 5.0°), volar–dorsal translation ($R^2 > 0.8$ and RMSE < 2.5 mm; except triquetrum), but they performed poorly in predicting radial-ulnar and DPT ($0.3 < R^2 < 0.9$, and RMSE < 3.1 mm), and supination-pronation ($R^2 < 0.6$ and RMSE < 8°). The mean errors (which reflect the overall bias of the models) were submillimeter or sub-degree for all predicted DOFs and carpal bones—except supination-pronation of the capitate, which had a bias of −1.2° (Table 2 and Supplementary Figs. S2.1-6). All quadratic surface parameters are available in Supplementary Table S1.

The Delaunay visualization of the carpal bone kinematics, the mathematical model, and the model's error demonstrated that the model performed well in the mid-region (i.e., mid-FE and mid-RU) of wrist positions, and it performed less well at the extreme range of motions where fewer data were available (Fig. 4; SCA$_{FE}$ as a representative, the rest can be observed in [Supplementary
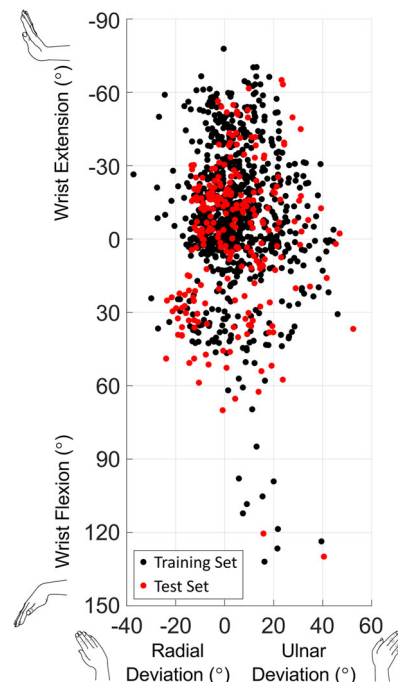
Figure 3. Training set (motions used to construct the model) from 86 wrists and test set (motions used to evaluate the model) from 30 wrists were randomly selected from the database. Each data point has 42 other dimensions for seven carpal bones and 6 degrees-of-freedom [Color figure can be viewed at wileyonlinelibrary.com]

Table 2. Root-Mean-Square Error (RMSE), R^2, and Model Error's Bias of 40 Second-Order Algebraic Fit to Every DOFs on the Test Set (20 Subjects, 30 Wrists)

Bone	Root Mean Square Error (RMSE)					
	SP (°)	FE (°)	RU (°)	DPT (mm)	RUT (mm)	VDT (mm)
Capitate	5.2	–	–	1.2	1.1	1.8
Scaphoid	3.5	4.2	3.2	0.9	1.1	1.1
Lunate	3.6	5.9	3.6	0.9	1.2	1.0
Hamate	5.2	3.1	2.2	1.4	1.4	2.3
Triquetrum	4.3	6.0	3.8	1.5	1.5	1.6
Trapezoid	7.3	4.0	5.0	2.0	3.1	2.5
Trapezium	6.0	2.7	4.8	1.8	2.9	2.1

Bone	R^2					
	SP	FE	RU	DPT	RUT	VDT
Capitate	0.2	–	–	0.9	0.9	0.9
Scaphoid	0.5	1.0	0.7	0.8	0.7	0.9
Lunate	0.3	0.9	0.6	0.7	0.5	0.8
Hamate	0.2	1.0	1.0	0.8	0.9	0.8
Triquetrum	0.6	0.9	0.7	0.5	0.3	0.3
Trapezoid	0.2	1.0	0.9	0.7	0.6	0.8
Trapezium	0.2	1.0	0.9	0.7	0.8	0.8

Bone	Model Error's Bias					
	SP (°)	FE (°)	RU (°)	DPT (mm)	RUT (mm)	VDT (mm)
Capitate	−1.2	–	–	0.1	0.1	0.0
Scaphoid	−0.3	0.1	−0.3	0.1	-0.1	0.0
Lunate	−0.1	0.0	−0.5	0.0	-0.1	−0.1
Hamate	−0.9	0.3	0.2	0.2	0.2	−0.1
Triquetrum	−0.5	−0.2	−0.1	0.0	0.0	−0.2
Trapezoid	−0.5	−0.2	−0.4	0.3	-0.2	0.2
Trapezium	−0.5	0.0	−0.7	0.2	-0.4	0.0

Degrees-of-freedoms are supination–pronation (SP), flexion–extension (FE), radial–ulnar deviation (RU), distal–proximal translation (DPT), radial–ulnar translation (RUT), and volar–dorsal translation (VDT). Translations RMSE is scaled back by the cube root of the average capitate volume (~3,700 mm³) for a better demonstration of RMSEs.

Fig. S3.1-42]). The histogram of errors of the mathematical model based on the position of the wrist revealed that the model error was normally distributed for all models and DOFs, except supination-pronation (Supplementary Fig. S4.1-42 and Supplementary Table S2.1-2). For example, for the SCA_{FE}, the bias of $<1°$, and the standard deviation of $<5°$ was calculated for all octants (Fig. 5; scaphoid FE as a representative).

The wrist's FE/RU ratio of the MM wrist path (MM slope) of each bone and DOF demonstrated different patterns of wrist movement for the bones in the proximal and distal carpal row (Fig. 6). The MM slopes were statistically different between proximal and distal rows in both FE and VDT ($p < 0.01$) (Table 3). The MM slopes for FE were close to 0 for all bones in the distal row (hamate, trapezoid, and trapezium), while they were between 0.6 and 1.2 for the proximal row bones (triquetrum, lunate, and scaphoid) (Table 3). The same comparison for VDT demonstrated a −0.3 to 0.3 range

for the bones in the distal row and 1.1–1.7 range for the bones in the proximal row. MM wrist paths for RUT and RU were not linear, thus they were compared at incremental wrist positions, and showed the paths occurred at different positions of the wrist for bones in a proximal and distal row. For instance, the MM wrist path in RU for the hamate, trapezoid, and triquetrum had a wrist RU of $<4°$ at a flexion angle of 100°, reduced to 0° at the neutral pose, and increased to $<3°$ wrist RU at extension angle of 80°. For triquetrum, lunate, and scaphoid the path occurred at a much larger wrist RU, which went from 15° in flexion to 0 at neutral, and about 40° in extension (Fig. 6). Because of the weaker prediction of the model for PS and PDT, the MM wrist paths were not compared in those DOFs.

DISCUSSION
The purposes of this study were to assemble a large database of in vivo wrist motions, to construct mathematical
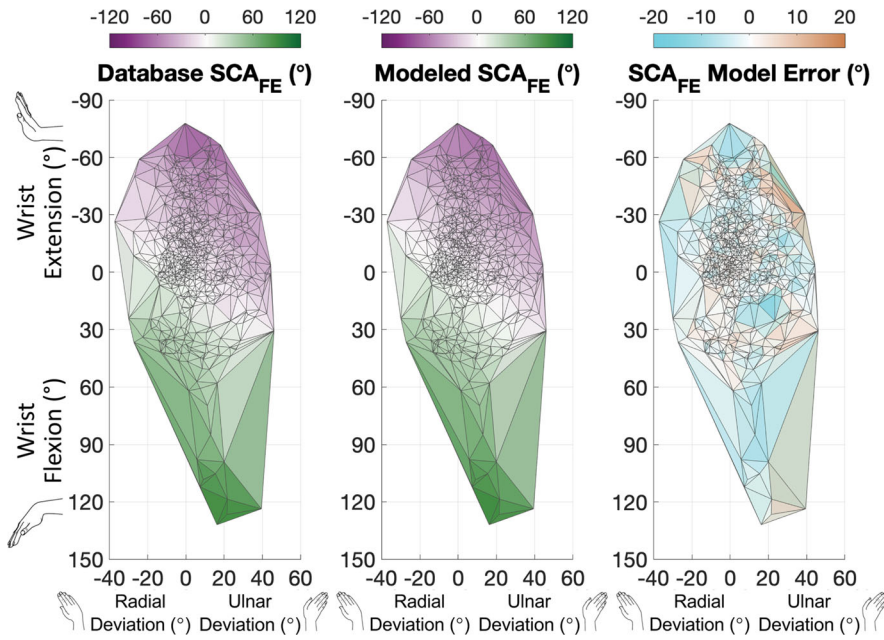
Figure 4. The flexion–extension of scaphoid (SCA_{FE}) as the function of wrist motion for the database (Left), quadratic model's prediction (Middle), and the model error (Right). The model error (the differences between the training values and predicted values) qualitatively demonstrate a similar model performance in all regions. Each triangle's face color is the average of the SCA_{FE} at each vertex [Color figure can be viewed at wileyonlinelibrary.com]

models that predict carpal bone kinematics as a function of wrist FE and RU using the database, and to determine the wrist motion paths that generated minimal motions for each of the carpal bones. The predictive quadratic models were developed using a subset of the database as a training set, and they were validated using the remainder of the database as a test set. The models' predictions were best on the test set for FE, RU, and VDT DOFs. The models demonstrated that the minimal motion paths of the distal carpal row (hamate, capitate, trapezoid, and trapezium) were different than the minimal motion paths of the proximal row (triquetrum, lunate, and scaphoid). The path was along the anatomical axis of wrist motion for bones of the distal row, while it was oblique to the main axis (in a dart-thrower's plane) for the bones of the proximal row.

3D understanding of individual carpal bone motion as the wrist moves in different motion paths is needed for clinicians to diagnose and deliver effective solutions for patients following injury or disease. The current open-source database, the GUI available with it, and the mathematical model constructed in this study, allows one to observe carpal bone articulations within a relatively large population both quantitatively and visually. In addition, similar to the grand challenge competition to predict in vivo knee loads,[48] investigators can use the current database to construct elaborate models to predict the kinematics of individual carpal bones using more complex mathematical models, bone shapes, or finite element models.

Our model demonstrates that the bones of the distal and proximal rows move minimally during two distinct wrist motion paths (one along the anatomical axes of wrist motion, and the other oblique to the main axis), but it does not explicitly prove or disprove any particular theory of carpal bone motion that has been developed to date.[6,12,13] The row theory[7–9,49] described the kinematics of the wrist with two rows organized proximally (lunate and triquetrum) and distally (hamate, capitate, trapezoid, and trapezium), having the scaphoid as a bridge or connection between these two rows. Our mathematical model confirmed that the hamate-capitate-trapezoid-trapezium complex moves relatively rigidly (within 3°), similar to the row theory and previous studies;[13,26] however, our model demonstrated more variability of motion among the bones of the proximal row. Thus, to consider the bones of the proximal row as part of a rigid element would not be an accurate interpretation of this dataset. Further studies using the database and mathematical modeling will be required to evaluate the previous carpal theories or examine new ones.

To develop carpal bone kinematic models as a function of the wrist motion, we made some assumptions about the motion's definition and model's specification. We used the wrist motion computed from the subject's neutral position to remove the shape variation of the carpal bones from the model generation process. While this assumption enables us to devise a clinically relevent model, it ignores the variation in positioning of the subjects' wrists at the neutral posture. The neutral position's variation can be calculated by looking at the capitate's posture (as an alternative to the third metacarpal), and it was within a 95% confidence interval of ~10° in our database. However, this interval is an approximation because it also depends upon the ICS definition of the capitate, which varies with the bone shape. Future investigation can focus on generating a landmark-based coordinate system for individual carpal bones to evaluate this effect or to generate posture-based predictive models. Additionally, the offset in the
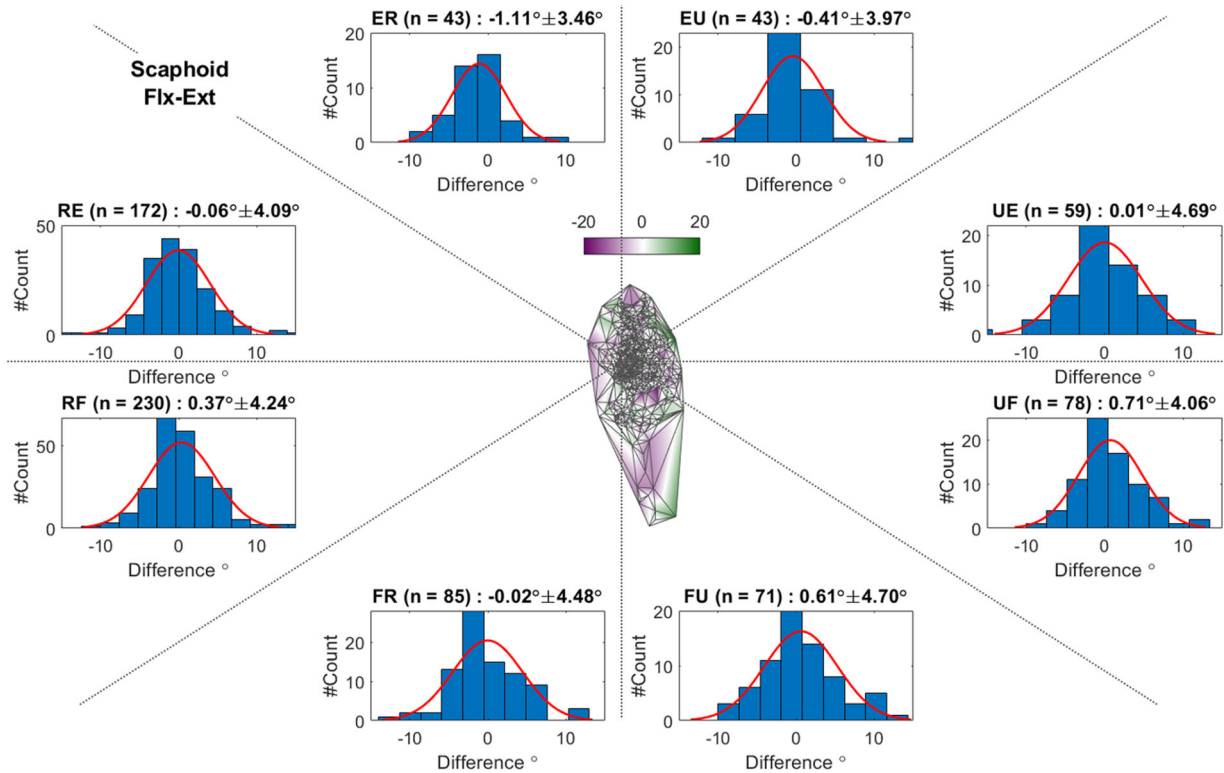
Figure 5. Mathematical model errors for scaphoid flexion–extension (SCA$_{FE}$), the histogram of errors based on the wrist movement for each octant of radial–ulnar (RU) and FE. The middle figure shows the model error across kinematics space, and every histogram shows the errors in every subdivision. The octants are defined based on the relationship between radial (R)/ulnar (U) deviation and flexion (F)/extension (E) of the wrist. For example, UE defines the region that the ulnar deviation is larger than extension, and FR describes the region that flexion is larger than the radial deviation [Color figure can be viewed at wileyonlinelibrary.com]
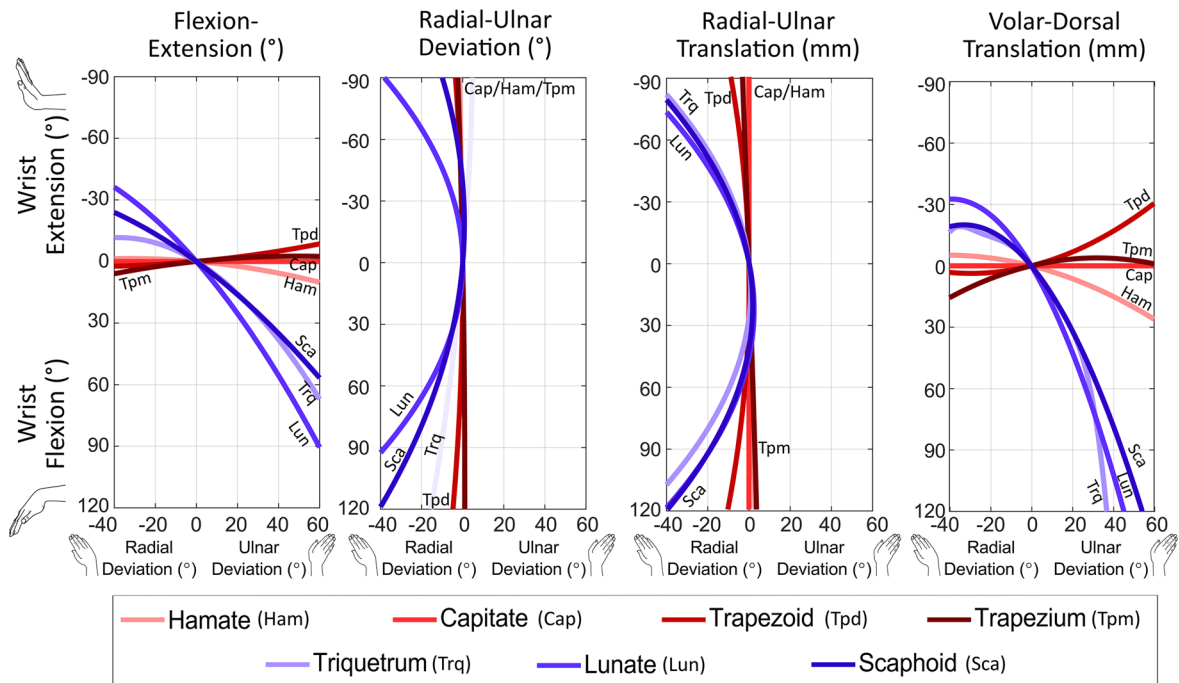
Figure 6. Wrist paths that generate minimal flexion–extension, radial–ulnar deviation, radial–ulnar translation, and volar–dorsal translation of carpal bones. Different patterns of wrist paths were seen for the carpal bones in the distal row (i.e., hamate, capitate, trapezoid, and trapezium) and proximal row (i.e., triquetrum, lunate, and scaphoid) [Color figure can be viewed at wileyonlinelibrary.com]

Table 3. The Lower Confidence Interval (LCI) and Upper Confidence Interval (UCI) of the Slope of the Path That Generates a Minimal Carpal Bone Motion (MM Slope)

Flexion–Extension MM Slope's CI			Volar Dorsal Translation MM Slope's CI		
Bone	LCI	UCI	Bone	LCI	UCI
Hamate	0.09	0.11	Hamate	0.2	0.3
Trapezoid	−0.09	−0.08	Trapezoid	−0.3	−0.2
Trapezium	−0.1	−0.09	Trapezium	−0.3	−0.2
Triquetrum	0.6	0.7	Triquetrum	1.1	1.3
Lunate	1.1	1.2	Lunate	1.5	1.7
Scaphoid	0.7	0.8	Scaphoid	1.1	1.3

Linear regression was used to calculate the MM Slope. The comparison for flexion–extension (FE) and volar–dorsal translation (VDT) revealed different patterns of wrist movement that generates minimal motions for the bones in the proximal row (slopes < 0.3), and the bones in the distal row (slopes > 0.6) of carpal bones.

mathematical model was fixed to zero with the underlying assumption that carpal bones orientation in the neutral pose is similar for all subjects. This assumption was ascertained by attaining minimal and approximately zero offsets, when the offsets were accounted for in training the models. Moreover, to construct the mathematical model, we chose the simplest model that was reasonably accurate with close to zero overall mean error. A first-order equation was incapable of predicting the extreme positions; thus, by increasing the degrees to a second-order algebraic equation, we were able to model the extreme range-of-motion points, as well as keep the model relatively simple. More complex models would likely achieve higher accuracy. We also assumed that all DOFs are independent in training our mathematical model and multivariate regression models might yield to a higher accuracy prediction.

We did not evaluate the collisions between the carpal bones in this study. Consideration of carpal bone collision using finite element modeling might yield higher accuracy with a refined model. Additionally, it has been shown that the lunate has two main anatomical shapes, and two different motion paths have been proposed for it;[50] we did not consider effects of bone shapes in our modeling (although we accounted for the size by scaling all carpal bones). Further studies need to examine the influence of the differing shapes of carpal bones on the wrist kinematics. In our model, we did not include variables, such as sex, age group, and sidedness, because they were out of the scope of this study's purpose; although, it has been shown that these variables are not associated with the kinematics after scaling the translation by the cubic root of the volume of the capitate.[46] Lastly, our model was not a good predictor for pronosupination of any of the carpal bones, which was most likely because the wrist was considered as a two-DOF system without any

pronosupination, as well as the limited supination-pronation of carpal bones that is generally <5° across all wrist positions.[19]

The expanded database and mathematical model constructed from this study should facilitate clinical visualization of normal and pathological wrist motion patterns (using the GUI) and will enable investigators to analyze the kinematics of the wrist joint and the articulations of its carpal bones. The GUI created in this study can accommodate subject-specific bone models to incorporate kinematic data (actual observed values or modeled kinematics) to visualize different motions to the user. As a secondary goal, our model demonstrated that the pattern of wrist motion that generates minimal motion for the distal row of carpal bones (i.e., hamate, capitate, trapezoid, and trapezium) is different than that of for the proximal row bones (i.e., triquetrum, lunate, and scaphoid).

AUTHOR'S CONTRIBUTION
B.A. was involved in analyzing and interpreting the data, as well as drafting the manuscript. D.H.L. was involved with advising on data analysis, interpreting the data, as well as critical revising of the paper. D.C.M., A-P.C.W., E.A., and S.W.W. were instrumental in acquiring and reducing the raw data from all studies, and critically revising of the paper. J.J.C. was involved with designing the study acquiring and reducing the raw data from all studies, interpreting the data, and critically revising the manuscript. All authors provided feedback and edited the manuscript. All authors have approved the final submitted manuscript.

REFERENCES
1. Lam KS, Woodbridge S, Burke FD. 2003. Wrist function after excision of the pisiform. J Hand Surg Br Eur 28:69–72.
2. Patterson RM, Williams L, Andersen CR, et al. 2007. Carpal kinematics during simulated active and passive motion of the wrist. J Hand Surg Am 32:1013–1019.
3. Nanno M, Buford WL, Patterson RM, et al. 2006. Three-dimensional analysis of the ligamentous attachments of the first carpometacarpal joint. J Hand Surg Am 31:1160–1170.
4. Moojen TM, Snel JG, Ritt MJ, et al. 2002. Scaphoid kinematics in vivo. J Hand Surg Am 27:1003–1010.
5. Horii E, An KN, Linscheid RL. 1993. Excursion of prime wrist tendons. J Hand Surg Am 18:83–90.
6. Rainbow MJ, Wolff AL, Crisco JJ, et al. 2016. Functional kinematics of the wrist. J Hand Surg Eur 41:7–21.

7. Bryce TH. 1896. Certain points in the anatomy and mechanism of the wrist-joint reviewed in the light of a series of rontgen ray photographs of the living hand. J Anat Physiol 31:59–79.

8. Destot E. 1986. The classic. Injuries of the wrist. A radiological study. By Etienne Destot. 1926. Clin Orthop 202:3–11. Translated by Atkinson, F.R.B.

9. Fick R. 1911. Handbuch der Anatomie und Mechanik der Gelenke unter Berucksichtigung der Bewegenden Muskein. Jena: Fischer.

10. Landsmeer JM. 1961. Studies in the anatomy of articulation. I. The equilibrium of the "intercalated" bone. Acta Morphol Neerl Scand 3:287–303.

11. Linscheid RL, Dobyns JH, Beabout JW, et al. 1972. Traumatic instability of the Wrist: diagnosis, classification, and pathomechanics. J Bone Joint Surg 54:1612–1632.

12. Navarro A. 1921. Luxaciones del carpo. Anales de la Facultad de. Medicina 6:113–141.

13. Taleisnik J. 1976. The ligaments of the wrist. J Hand Surg Am 1:110–118.

14. MacConaill MA. 1941. The mechanical anatomy of the carpus and its bearings on some surgical problems. J Anat 75:166–175.

15. Garcia-Elias M. 1997. Kinetic analysis of carpal stability during grip. Hand Clin 13:151–158.

16. Craigen MA, Stanley JK. 1995. Wrist kinematics. Row, column or both? J Hand Surg Br 20:165–170.

17. Carelsen B, Bakker NH, Strackee SD, et al. 2005. 4D rotational x-ray imaging of wrist joint dynamic motion. Med Phys 32:2771–2776.

18. Choi YS, Lee YH, Kim S, et al. 2013. Four-dimensional real-time cine images of wrist joint kinematics using dual source CT with minimal time increment scanning. Yonsei Med J 54:1026–1032.

19. Crisco JJ, Coburn JC, Moore DC, et al. 2005. In vivo radiocarpal kinematics and the dart thrower's motion. J Bone Joint Surg 87:2729–2740.

20. Kobayashi M, Berger RA, Nagy L, et al. 1997. Normal kinematics of carpal bones: a three-dimensional analysis of carpal bone motion relative to the radius. J Biomech 30:787–793.

21. Moritomo H, Apergis EP, Herzberg G, et al. 2007. 2007 IFSSH committee report of wrist biomechanics committee: biomechanics of the so-called dart-throwing motion of the wrist. J Hand Surg Am 32:1447–1453.

22. Akhbari B, Morton AM, Moore DC, et al. 2019. Kinematic accuracy in tracking total wrist arthroplasty with biplane videoradiography using a computed tomography-generated model. J Biomech Eng 141:044503.

23. Halilaj E, Rajagopal A, Fiterau M, et al. 2018. Machine learning in human movement biomechanics: best practices, common pitfalls, and new opportunities. J Biomech 81:1–11.

24. Werner FW, Short WH, Green JK. 2005. Changes in patterns of scaphoid and lunate motion during functional arcs of wrist motion induced by ligament division. J Hand Surg Am 30:1156–1160.

25. Werner FW, Short WH, Fortino MD, et al. 1997. The relative contribution of selected carpal bones to global wrist motion during simulated planar and out-of-plane wrist motion. J Hand Surg Am 22:708–713.

26. Sandow MJ, Fisher TJ, Howard CQ, et al. 2014. Unifying model of carpal mechanics based on computationally derived isometric constraints and rules-based motion—the stable central column theory. J Hand Surg Eur Vol 39:353–363.

27. Gislason MK, Stansfield B, Nash DH. 2010. Finite element model creation and stability considerations of complex biological articulation: the human wrist joint. Med Eng Phys 32:523–531.

28. Carrigan SD, Whiteside RA, Pichora DR, et al. 2003. Development of a three-dimensional finite element model for carpal load transmission in a static neutral posture. Ann Biomed Eng 31:718–725.

29. Gíslason MK, Nash DH 2012. Finite element modelling of a multi-bone joint: the human wrist. finite element analysis—new trends and developments. Available from: https://www.intechopen.com/books/finite-element-analysis-new-trends-and-developments/finite-element-modelling-of-a-multi-bone-joint-the-human-wrist

30. Moore DC, Crisco JJ, Trafton TG, et al. 2007. A digital database of wrist bone anatomy and carpal kinematics. J Biomech 40:2537–2542.

31. Crisco JJ, Coburn JC, Moore DC, et al. 2005. Carpal bone size and scaling in men versus in women. J Hand Surg Am 30:35–42.

32. Coburn JC, Upal MA, Crisco JJ. 2007. Coordinate systems for the carpal bones of the wrist. J Biomech 40:203–209.

33. Neu CP, Crisco JJ, Wolfe SW. 2001. In vivo kinematic behavior of the radio-capitate joint during wrist flexion-extension and radio-ulnar deviation. J Biomech 34:1429–1438.

34. Crisco JJ, Patel T, Halilaj E, et al. 2015. The envelope of physiological motion of the first carpometacarpal joint. J Biomech Eng 137:101002.

35. Kamal RN, Rainbow MJ, Akelman E, et al. 2012. In vivo triquetrum-hamate kinematics through a simulated hammering task wrist motion. J Bone Joint Surg Am 94:e85.

36. Leventhal EL, Moore DC, Akelman E, et al. 2010. Carpal and forearm kinematics during a simulated hammering task. J Hand Surg Am 35:1097–1104.

37. Rainbow MJ, Kamal RN, Moore DC, et al. 2015. Subject-specific carpal ligament elongation in extreme positions, grip, and the Dart Thrower's motion. J Biomech Eng 137:111006.

38. Rainbow MJ, Kamal RN, Leventhal E, et al. 2013. In vivo kinematics of the scaphoid, lunate, capitate, and third metacarpal in extreme wrist flexion and extension. J Hand Surg Am 38:278–288.

39. Rainbow MJ, Crisco JJ, Moore DC, et al. 2012. Elongation of the dorsal carpal ligaments: a computational study of in vivo carpal kinematics. J Hand Surg Am 37:1393–1399.

40. Halilaj E, Moore DC, Patel TK, et al. 2014. Thumb carpometacarpal joint congruence during functional tasks and thumb range-of-motion activities. Conf Proc IEEE Eng Med Biol Soc 2014:4354–4357.

41. Halilaj E, Rainbow MJ, Got C, et al. 2014. In vivo kinematics of the thumb carpometacarpal joint during three isometric functional tasks. Clin Orthop Relat Res 472:1114–1122.

42. Moore DC, Halilaj E, Patel TK, et al. 2014. Computed tomography image-based kinematic analysis: an overview. In: Neu CP, Genin GM, editors. Handbook of imaging in biological mechanics, 1st ed. Boca Raton, FL: CRC Press. p 115–126. Available from: http://www.crcnetbase.com/doi/abs/10.1201/b17566-14

43. Marai GE, Laidlaw DH, Crisco JJ. 2006. Super-resolution registration using tissue-classified distance fields. IEEE Trans Med Imaging 25:177–187.

44. Crisco JJ, Pike S, Hulsizer-Galvin DL, et al. 2003. Carpal bone postures and motions are abnormal in both wrists of patients with unilateral scapholunate interosseous ligament tears. J Hand Surg Am 28:926–937.

45. Wu G, van der Helm FCT, (DirkJan) Veeger HEJ, et al. 2005. ISB recommendation on definitions of joint coordinate systems of various joints for the reporting of human joint motion—Part II: shoulder, elbow, wrist and hand. J Biomech 38:981–992.

46. Rainbow MJ, Crisco JJ, Moore DC, et al. 2008. Gender differences in capitate kinematics are eliminated after accounting for variation in carpal size. J Biomech Eng 130:041003.

47. Lee DT, Schachter BJ. 1980. Two algorithms for constructing a Delaunay triangulation. Int J Comput Inf Sci 9:219–242.

48. Fregly BJ, Besier TF, Lloyd DG, et al. 2012. Grand challenge competition to predict in vivo knee loads. J Orthop Res 30:503–513.

49. Kauer JMG. 1986. The mechanism of the carpal joint. Clin Orthop Relat Res 16–26.

50. Abe S, Moritomo H, Oka K, et al. 2018. Three-dimensional kinematics of the lunate, hamate, capitate and triquetrum with type 1 or 2 lunate morphology. J Hand Surg Eur Vol 43:380–386.

SUPPORTING INFORMATION

Additional supporting information may be found in the online version of this article.